Communication

Simulation of 3-D Electromagnetic Scattering and Inverse Scattering by Arbitrary Anisotropic Dielectric Objects Embedded in Layered Arbitrary Anisotropic Media

Jianwen Wang, Jiawen Li, Yanjin Chen, Feng Han, and Qing Huo Liu

***Abstract*— This communication studies 3-D electromagnetic (EM) scattering and inverse scattering of arbitrary anisotropic dielectric objects embedded in multilayered media. Different from previous work, the scatterer is not only arbitrary anisotropic, but also the arbitrary anisotropy of the layered background media is formed by rotation of the principal axes of uniaxial media. In addition, the scatterers are allowed to be placed across layer boundaries. The forward model is formulated by the electric field integral equation (EFIE), solved by the biconjugate gradient stabilized (BCGS) method, and accelerated by the fast Fourier transform (FFT). The time complexity is analyzed for the BCGS-FFT applied to layered arbitrary anisotropic media. In the inversion model, the variational Born iterative method (VBIM) is employed to reconstruct the arbitrary anisotropic profiles of both the permittivity and conductivity. Numerical simulations are performed to verify the feasibility and antinoise ability of the forward and inverse solvers in the circumstance of layered arbitrary anisotropic background media.**

***Index Terms*— Arbitrary anisotropy, inverse scattering, multilayered media, scattering.**

I. Introduction

Electromagnetic (EM) scattering and inverse scattering have wide applications for near-surface detection [1], microwave imaging [2], geophysical prospecting [3], and so on. In past decades, great efforts have been contributed to both the algorithms and real-world measurements for scattering and inverse scattering. In the beginning, scatterers are placed in a homogeneous medium and scattered fields are collected to retrieve the dielectric parameters of the scatterers [4]. In such a scenario, the Green's function for the homogeneous background medium is readily evaluated. Typical applications include microwave imaging of unknown multiple objects [5], biomedical imaging [6], etc. Later, the planarly layered medium is considered. Layered medium Dyadic Green's functions (DGFs) are computed through Sommerfeld integration to account for the multiple reflections and transmission at layer boundaries [7]. One of the important applications of EM scattering in planarly layered media is the geophysical exploration. For example, the fast computation to simulate EM scattering of the oil reservoir, utility pipes, buried land mines, or unexploded ordnance is presented in [8] and [9]. In controlled-source EM (CSEM) measurements [10], [11], the background medium can be treated as a half-space model or horizontally layered. Other geophysical applications include hydraulic fracture evaluation [3], subsurface inspection by ground-penetrating radar (GPR) [12], through-wall-imaging (TWI) [13], and so on. However, in nature, some materials also show obvious anisotropy and thus it is necessary to study the effect of anisotropy on EM scattering.

Previously, a lot of research work has been accomplished for the EM scattering and/or inverse scattering in the circumstance of layered anisotropic background media. In [14] and [15], the background medium was uniaxial anisotropic with the optical axes perpendicular to the layer boundaries but the scatterers can be uniaxial or arbitrary anisotropic. The EM scattering cases in which the optical axes of the background medium are parallel to the layer boundaries were also studied [16]. On the other hand, the inversion of anisotropic scatterers embedded inside the layered uniaxial media was implemented recently [17], [18]. But the EM scattering in the layered arbitrary anisotropic media is rarely studied. Therefore, the focus of this communication is to investigate the scattering and inverse scattering of arbitrary anisotropic objects embedded in multilayered arbitrary anisotropic media. There are several possible applications of this research work. For example, in the geophysical exploration [19], the arbitrary anisotropic conductivity of the layered cross-bedded formation with symmetrical tensors is caused by the rotation of the principal axes. In the ionosphere remote sensing, the oblique geomagnetic field changes the perturbed region [20] from a layered gyrotropic medium with conjugate symmetric tensors to a layered arbitrary anisotropic medium [21]. In addition, in our work, the scatterer is allowed to be placed across multiple layers which is different from previous work [14], [15].

One of the commonly used methods to formulate the EM scattering problems is using the integral equations. The most direct way to solve the discretized integral equations is the method of moments (MoM). However, the computational cost of MoM is high. Fast solvers such as the adaptive integral method (AIM) [9] and the biconjugate gradient stabilized fast Fourier transform (BCGS-FFT) [15] are proposed to replace MoM to solve forward scattering problems. For the inverse scattering, many iterative methods such as contrast source inversion (CSI) [22], subspace-based optimization method (SOM) [23], and Born iterative method (BIM) and its variants [24] are validated in the previous work. CSI and SOM usually require good initial models to start the iteration. The variational BIM (VBIM) converges faster than BIM and needs less computation cost compared with distorted BIM (DBIM), and thus is adopted in this communication. It calls the forward solver BCGS-FFT iteratively to reconstruct the arbitrary anisotropic parameters of the dielectric scatterers.

The organization of this communication is as follows. In Section II, the evaluation of DGFs in the layered arbitrary anisotropic dielectric

Manuscript received November 7, 2019; revised January 9, 2020; accepted January 27, 2020. Date of publication February 14, 2020; date of current version August 4, 2020. This work was supported by the National Natural Science Foundation of China under Grant 41504120. *(Corresponding authors: Feng Han; Qing Huo Liu.)*

Jianwen Wang, Jiawen Li, Yanjin Chen, and Feng Han are with the Institute of Electromagnetics and Acoustics, Xiamen University, Xiamen 361005, China, and also with the Key Laboratory of Electromagnetic Wave Science and Detection Technology, Xiamen University, Xiamen 361005, China (e-mail: feng.han@xmu.edu.cn).

Qing Huo Liu is with the Department of Electrical and Computer Engineering, Duke University, Durham, NC 27708 USA (e-mail: qhliu@duke.edu).

Color versions of one or more of the figures in this communication are available online at http://ieeexplore.ieee.org.

Digital Object Identifier 10.1109/TAP.2020.2972636

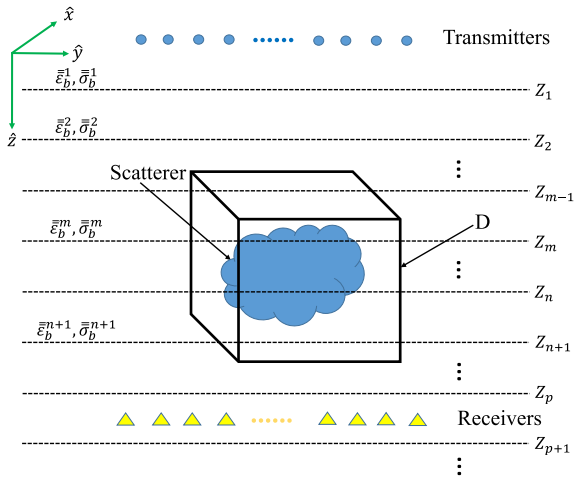

Fig. 1. Typical configuration for EM scattering in a planarly layered arbitrary anisotropic medium.

medium is discussed. Forward and inverse models are presented, and the FFT acceleration in the forward computation is analyzed. In Section III, the forward scattering of a cross-layer scatterer is simulated by BCGS-FFT and the results are compared with finite element method (FEM) by the commercial software COMSOL. Then, 12 anisotropic model parameters of the cross-layer scatterer are simultaneously reconstructed by VBIM, which is enhanced by the structural consistency constraint (SCC) and structural continuity scanning (SCS) algorithms. The hybrid method VBIM-SCC-SCS has been validated in our previous work [18] and will not be discussed in this communication. Then, the antinoise ability of the inversion is studied. In Section V, conclusions are presented.

II. Formulation

The objective of this communication is to solve the scattering and inverse scattering problems of 3-D arbitrary anisotropic dielectric objects embedded in a layered arbitrary anisotropic background medium. The typical configuration is shown in Fig. 1. We assume that the scatterer with arbitrary anisotropy for both permittivity and conductivity is placed across several layers and has the same permeability as that of free space μ_0. Its relative permittivity and conductivity tensors are written as

$$\overline{\overline{\varepsilon}}_s = \begin{bmatrix} \varepsilon^s_{11} & \varepsilon^s_{12} & \varepsilon^s_{13} \\ \varepsilon^s_{21} & \varepsilon^s_{22} & \varepsilon^s_{23} \\ \varepsilon^s_{31} & \varepsilon^s_{32} & \varepsilon^s_{33} \end{bmatrix}, \quad \overline{\overline{\sigma}}_s = \begin{bmatrix} \sigma^s_{11} & \sigma^s_{12} & \sigma^s_{13} \\ \sigma^s_{21} & \sigma^s_{22} & \sigma^s_{23} \\ \sigma^s_{31} & \sigma^s_{32} & \sigma^s_{33} \end{bmatrix} \tag{1}$$

where s denotes the scatterer, $\varepsilon^s_{pq} = \varepsilon^s_{qp}$, and $\sigma^s_{pq} = \sigma^s_{qp}$ with p, $q = 1$, 2, and 3. Although the proposed method is applicable to arbitrary anisotropic media with asymmetric tensors of the dielectric parameters, we only consider the symmetrical tensors rotated from uniaxial ones in this work, which is ubiquitous in nature [19]. For convenience, the complex relative permittivity tensor of the scatterer can be written as

$$\overline{\overline{\epsilon}}_s = \overline{\overline{\varepsilon}}_s + \frac{\overline{\overline{\sigma}}_s}{j\omega\varepsilon_0} \tag{2}$$

where ω is the angular frequency of the EM wave.

The arbitrary anisotropy of the ith layer of the background medium is constructed by rotating the principal axis of a uniaxial medium. Such a phenomenon is always seen in engineering applications such as the geophysical exploration [19]. Therefore, dielectric parameters of the ith layer of the background medium are

$$\overline{\overline{\varepsilon}}^i_b = \mathbf{R}\overline{\overline{\varepsilon}}^i_{b0}\mathbf{R}^T, \qquad \overline{\overline{\sigma}}^i_b = \mathbf{R}\overline{\overline{\sigma}}^i_{b0}\mathbf{R}^T \tag{3}$$

where the subscript b denotes the background, the superscript T means the matrix transpose, and $\mathbf{R}$ is the rotation transformation matrix whose details are given in [25, Appendix B]. $\overline{\overline{\varepsilon}}^i_{b0}$ and $\overline{\overline{\sigma}}^i_{b0}$ are uniaxial tensors and expressed as

$$\overline{\overline{\varepsilon}}^i_{b0} = \mathrm{diag}\{\varepsilon^i_x, \varepsilon^i_x, \varepsilon^i_z\}, \qquad \overline{\overline{\sigma}}^i_{b0} = \mathrm{diag}\{\sigma^i_x, \sigma^i_x, \sigma^i_z\}. \tag{4}$$

Obviously, $\overline{\overline{\varepsilon}}^i_b$ and $\overline{\overline{\sigma}}^i_b$ become full symmetrical tensors after rotation to represent the arbitrary anisotropic property. Similarly, the complex tensor of the background medium can be written as

$$\overline{\overline{\epsilon}}^i_b = \overline{\overline{\varepsilon}}^i_b + \frac{\overline{\overline{\sigma}}^i_b}{j\omega\varepsilon_0}. \tag{5}$$

A. Evaluation of DGFs in Layered Arbitrary Anisotropic Media

Since the integral equations are used to solve the EM scattering problems in this work, layered medium DGFs must be evaluated first. The most straightforward method is to decompose the EM waves excited by a point source into a series of plane waves by Fourier expansions in the spectral domain. In the next step, the reflection and transmission coefficients in multiple layers are computed for each plane wave component. And finally, integration is performed to sum all the plane wave components at the observation point subject to the multiple reflection and transmission. When the layered medium is isotropic or uniaxial anisotropic with the optical axis perpendicular to the layer boundaries, the 2-D integration in the spectral domain with respect to k_x and k_y can be further simplified into 1-D Sommerfeld integration with respect to k_ρ. The details can be found in [7]. However, when the layered medium is arbitrary anisotropic, the azimuthal symmetry does not hold anymore. As a result, the 2-D integration with respect to k_x and k_y must be performed in an infinitely large horizontal plane. The mathematical formulas and numerical validations have been presented in [26]. One should note that there is no cross-coupling between transverse electric (TE) and transverse magnetic (TM) waves when reflection or transmission occurs at layer boundaries of isotropic or uniaxial media. Therefore, the reflection or transmission coefficients for TE or TM plane waves are expressed by two independent complex numbers. By contrast, they are expressed by two 2×2 matrices when the layered medium is arbitrary anisotropic since the cross-coupling between type I and type II waves is obvious [26].

Another important issue we want to emphasize here is the decomposition of DGFs in the $\hat{z}$-direction. In previous work [1], [8], [9], [14], [15], the DGF $\overline{\overline{\mathbf{G}}}$ is decomposed into the "plus" and "minus" parts in the $\hat{z}$ direction to facilitate the computation of the interactions between DGFs and the equivalent current inside a certain horizontal layer. See [7, eqs. (62)–(65)] and [8, eq. (12)]. Unfortunately, such a decomposition is not valid when the medium is arbitrary anisotropic. We can imagine the simplest scenario in which two different homogeneous arbitrary anisotropic media are divided by an infinite large plane at $z = z_1$. A source point $\mathbf{r}' = (x', y', z')$ and a field point $\mathbf{r} = (x, y, z)$ are located in the lower half-space. A plane wave including both type I and type II waves and with the unit amplitude starts from $\mathbf{r}'$, hits the layer boundary at $z = z_1$, and is reflected back to $\mathbf{r}$. By referring to [26], it is not difficult to derive the type I downgoing wave at $\mathbf{r}$

$$\begin{aligned} A^-_1(z) = {} & R_{11}\exp\left[\lambda^+_1(z_1 - z') + \lambda^-_1(z - z_1)\right] \\ & + R_{12}\exp\left[\lambda^+_2(z_1 - z') + \lambda^-_1(z - z_1)\right] \end{aligned} \tag{6}$$

TABLE I
DIELECTRIC PARAMETERS OF THE SECOND LAYER, THIRD LAYER, AND THE SCATTERER

	ε_{11}	ε_{12}	ε_{13}	ε_{22}	ε_{23}	ε_{33}	σ_{11}	σ_{12}	σ_{13}	σ_{22}	σ_{23}	σ_{33}
Second layer	1.275	-0.130	-0.150	1.425	0.260	1.500	0.238	-0.065	-0.075	0.313	0.130	0.350
Third layer	1.887	-0.152	-0.175	2.062	0.303	2.150	0.450	-0.087	-0.100	0.550	0.173	0.600
Scatterer	2.500	0.500	0.200	2.700	0.600	3.000	0.900	0.300	0.200	1.100	0.450	1.300

Remark: the unit of σ is mS/m.

where λ is the eigenvalue to characterize plane wave propagation inside arbitrary anisotropic media [26], the superscripts $+$ and $-$ denote the upgoing and downgoing waves, respectively, and the subscript 1 or 2 means the type I or type II wave. R_{11} or R_{12} stands for the reflection coefficient at the boundary $z = z_1$ for type I wave generated from the incident wave of type I or type II. In the layered arbitrary anisotropic medium, R_{12} is not zero. λ_2^+ and λ_1^- are neither equal nor have the opposite signs. Therefore, A_1^- cannot be decomposed to the "minus" part including $z - z'$ and the "plus" part including $z + z'$. However, when the arbitrary anisotropy degenerates into uniaxial anisotropy, R_{12} becomes zero and λ_1^- and λ_1^+ are equal or have the opposite signs, A_1^- can be decomposed. See [7, eqs. (62)–(65)].

B. Forward Model

The forward model is formulated by the state equation

$$\mathbf{E}_{inc}(\mathbf{r}) = \mathbf{E}_{tot}(\mathbf{r}) - j\omega\varepsilon_0 \int_D \overline{\overline{\mathbf{G}}}_{\mathbf{EJ}}(\mathbf{r}, \mathbf{r}')(\overline{\overline{\epsilon}}_s(\mathbf{r}') - \overline{\overline{\epsilon}}_b(\mathbf{r}'))\mathbf{E}_{tot}(\mathbf{r}')d\mathbf{r}' \quad (7)$$

where $\mathbf{E}_{inc}$ is the incident field when the scatterer is absent while $\mathbf{E}_{tot}$ is the total field when the scatterer is present. $\overline{\overline{\mathbf{G}}}_{\mathbf{EJ}}$ is the DGF in layered arbitrary anisotropic media [26] linking the source point $\mathbf{r}'$ and the field point $\mathbf{r}$. Apply (7) to $\mathbf{r}$ in D and discretize (7) to obtain the weak forms. And then, the BCGS-FFT method can be used to solve the total field $\mathbf{E}_{tot}$. Similar works have been accomplished in [14] and [15] for uniaxial media. Compared with these previous works, the forward computation in this work has following difference.

1) A point-matching procedure is adopted to transform (7) into matrix equations. The rooftop basis functions are not used.
2) The computation domain D is allowed to cross multiple layers, i.e., the equivalent current can distribute in several arbitrary anisotropic layers continuously.
3) The FFT acceleration for the interaction between the DGFs and equivalent current can only be applied in the horizontal xy plane. In the $\hat{z}$-direction, the DGF cannot be decomposed into the "plus" and "minus" parts. Consequently, the integration cannot be converted into FFT operations. This accordingly leads to the increase of the computation complexity. Suppose the computation domain D is divided into $N = N_x \times N_y \times N_z$ discretized cells. Compared with the BCGS-FFT solver in layered isotropic or uniaxial media [8], [15], the computation complexity increases to $O(KN_zNlog(N_xN_y))$, where K is the iteration number.

C. Inversion Model

The inversion model is formulated by the data equations

$$\mathbf{E}_{sct}(\mathbf{r}) = j\omega\varepsilon_0 \int_D \overline{\overline{\mathbf{G}}}_{\mathbf{EJ}}(\mathbf{r}, \mathbf{r}')(\overline{\overline{\epsilon}}_s(\mathbf{r}') - \overline{\overline{\epsilon}}_b(\mathbf{r}'))\mathbf{E}_{tot}(\mathbf{r}')d\mathbf{r}' \quad (8a)$$

$$\mathbf{H}_{sct}(\mathbf{r}) = j\omega\varepsilon_0 \int_D \overline{\overline{\mathbf{G}}}_{\mathbf{HJ}}(\mathbf{r}, \mathbf{r}')(\overline{\overline{\epsilon}}_s(\mathbf{r}') - \overline{\overline{\epsilon}}_b(\mathbf{r}'))\mathbf{E}_{tot}(\mathbf{r}')d\mathbf{r}' \quad (8b)$$

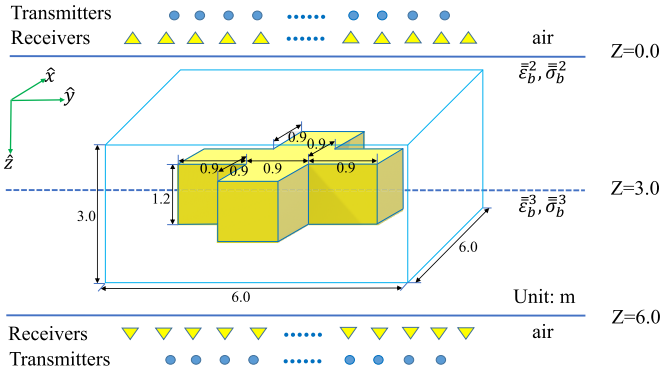

Fig. 2. Configuration of a cross shape scatterer embedded in a layered arbitrary anisotropic background medium.

where $\mathbf{E}_{sct}$ and $\mathbf{H}_{sct}$ are the scattered fields measured at the field point $\mathbf{r}$. In the inverse scattering computation, the source points $\mathbf{r}'$ and field points $\mathbf{r}$ are not overlapped, (8) is discretized, and 12 model parameters contained in $\overline{\overline{\epsilon}}_s$ are retrieved by VBIM-SCC-SCS simultaneously [18].

III. FORWARD SCATTERING VALIDATION

In this section, we validate the forward BCGS-FFT solver via comparing the results with numerical simulations of FEM by the commercial software COMSOL. The perfect-matched layers are adopted in the FEM computation. All the computation and simulations are performed on a workstation with 48-core Xeon E52697 v2 2.7G CPU, 512 GB RAM. The configuration for an arbitrary anisotropic cross shape scatterer embedded in a four-layer arbitrary anisotropic background medium is shown in Fig. 2. The top and bottom layers are air in which the transmitter and receiver arrays are placed. Two 4×4 transmitter arrays with the size of 18 m $\times$ 18 m are placed at $z = -3.0$ m and $z = 9.0$ m, respectively. Each transmitter is a unit dipole, operating at 30 MHz and polarized in the direction of (1, 1, 1). Two 5×5 receiver arrays with the size of 30 m $\times$ 30 m are placed at $z = -1.5$ m and $z = 7.5$ m, respectively. The scatterer is a cross shape, embedded in the second layer and the third layer, formed by cutting four small cuboids with the size of 0.9 m $\times$ 0.9 m $\times$ 1.2 m out of a rectangular shape with the dimensions of 2.7 m $\times$ 2.7 m $\times$ 1.2 m. The centers of the four cuboids and the rectangular shape are at (−1.05, −0.15, 3) m, (1.05, −0.15, 3) m, (−0.15, −1.05, 3) m, (-0.15, 1.05, 3) m, and (−0.15, −0.15, 3) m, respectively.

The dielectric parameters of the second and third arbitrary anisotropic layers and the scatterer are listed in Table I. The computation domain of BCGS-FFT with the dimensions of 6 m $\times$ 6 m $\times$ 3 m enclosing the scatterer has the center at (0, 0, 3.0) m. The electrical size of the scatterer is around half wavelength. For comparisons of total fields, we choose the transmitter at (0, 0, −3) m and two sets of 6×6 uniform sampling points with the spatial step of 0.9 m in both the $\hat{x}$- and

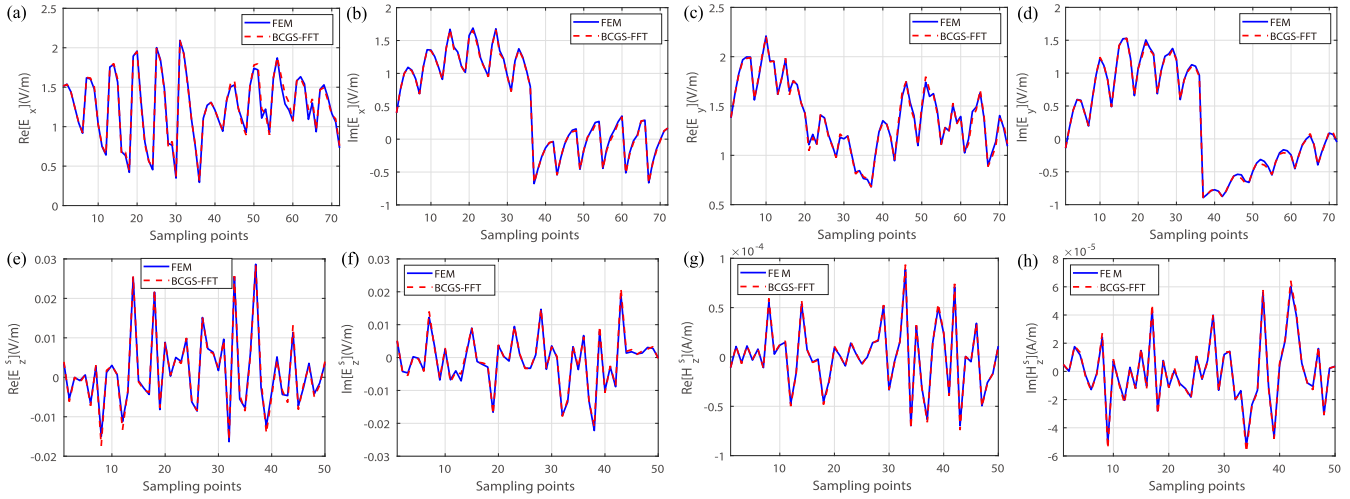

Fig. 3. Comparisons of the total electric fields in the domain D and the scattered fields at the receiver array solved by BCGS-FFT and simulated by FEM. (a) Real parts of total fields E_x. (b) Imaginary parts of total fields E_x. (c) Real parts of total fields E_y. (d) Imaginary parts of total fields E_y. (e) Real parts of scattered fields E_z. (f) Imaginary parts of scattered fields E_z. (g) Real parts of scattered fields H_z. (h) Imaginary parts of scattered fields H_z.

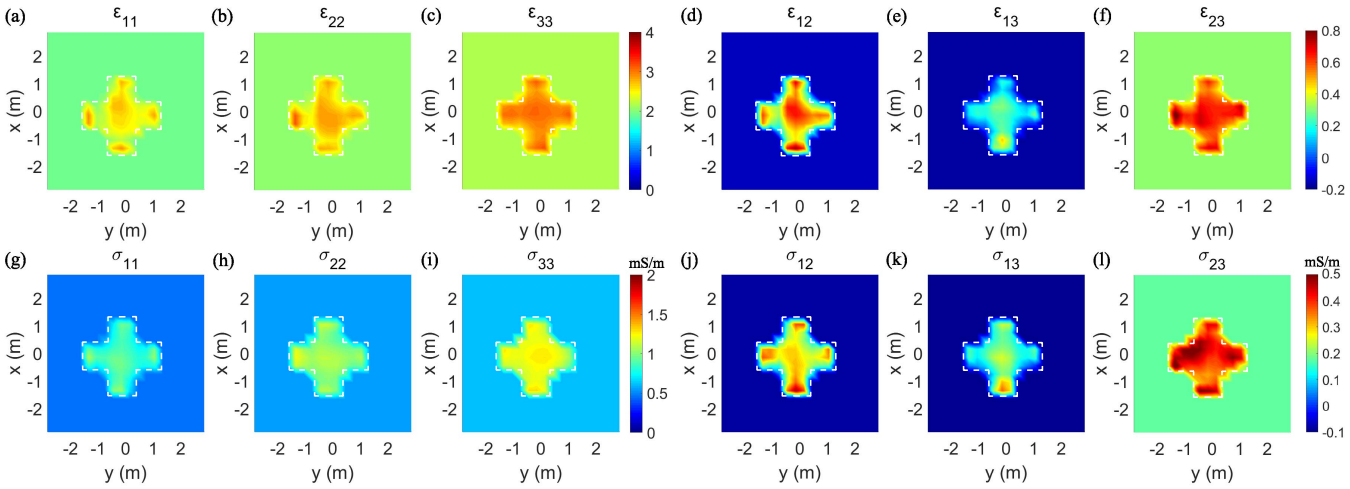

Fig. 4. 2-D xy slices of reconstructed results for the cross shape object by VBIM. (a)–(f) are slices at $z = 3.45$ m for the relative permittivity. (g)–(l) are slices at $z = 3.45$ m for the conductivity. The dotted boxes denote the true location of the scatterer.

$\hat{y}$-directions and located at $z = 2.25$ m and $z = 3.45$ m in the inversion domain. For scattered field comparisons, the field values are sampled at all the 50 receivers.

The BCGS-FFT iteration converges after six steps with the residual error of 5.79×10^{-6}. Fig. 3 shows the comparisons of the x-component and y-component of the total electric fields inside the computation domain and z-component of the scattered fields at the receiver array. The results show that the solutions of BCGS-FFT match the results of FEM well. The comparisons of the other components have the same good match and are not shown here. However, the BCGS-FFT has the obvious speed advantage over FEM. The BCGS-FFT spends around 1 min to complete the six iterations, while the simulation in COMSOL by FEM needs 19 min.

IV. Inversion Assessment

In this section, we reconstruct the anisotropic model parameters of the cross shape scatterer given in the forward computation in Section V. Twelve model parameters are retrieved simultaneously. The inversion domain is the same as the computation domain in the forward computation. It is divided into $20 \times 20 \times 10$ cubic cells and the size of each cubic cell is $\Delta x = \Delta y = \Delta z = 0.3$ m. Because each cell has 12 unknowns, there are totally 48 thousand unknowns to be reconstructed. We perform the inversion by VBIM-SCC-SCS and it terminates after 21 iterations when the relative residual error (RRE) of the reconstructed scattered field compared with the measured data is less than the threshold 5×10^{-4}. The 2-D xy slices and xz slices of the restructured anisotropic dielectric parameters of the cross shape scatterer are shown in Figs. 4 and 5, respectively. The true location and shape are illustrated by white dotted boxes. We can see that both the shape and 12 dielectric parameters of the scatterer are well reconstructed.

We then verify the antinoise ability of VBIM-SCC-SCS for the reconstruction of arbitrary anisotropic scatterers embedded in layered arbitrary anisotropic background media. The white Gaussian noise with a power signal-to-noise ratio (SNR) of 30 dB is added to the simulated scattered field. When the VBIM-SCC-SCS inversion procedure terminates after 15 iterations, the RRE is 4.763% for SNR = 30 dB. The detailed 2-D xy slices of the reconstructed results are shown in Fig. 6. We only show the xy slices of the diagonal elements. Other retrieved parameters and slices are similar

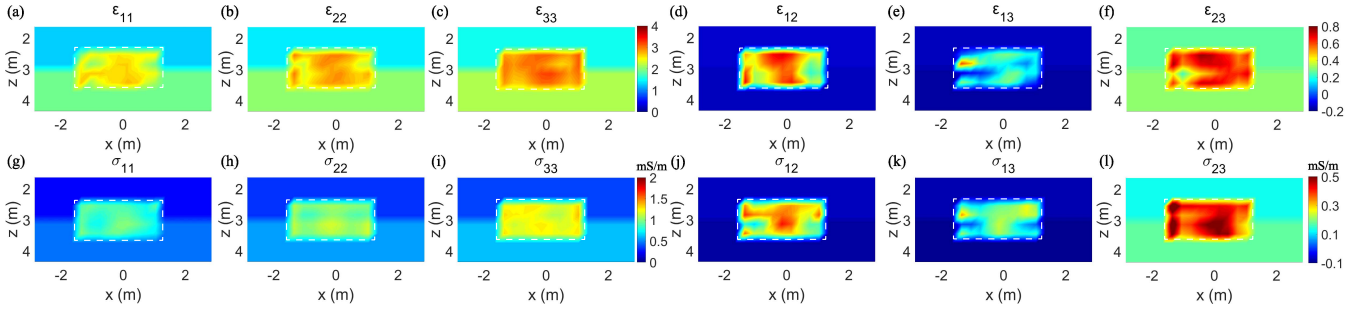

Fig. 5. 2-D xz slices of reconstructed results for the cross shape object by VBIM. (a)–(f) are slices at $y = -0.45$ m for the relative permittivity. (g)–(l) are slices at $y = -0.45$ m for the conductivity. The dotted boxes denote the true location of the scatterer.

TABLE II
MISFITS FOR VBIM-SCC-SCS WITHOUT NOISE AND WITH NOISE FOR THE CROSS SHAPE SCATTERER

SNR \ Misfit	Data misfit (%)	Model misfit (%)											
Parameter	Scattered fields	ε_{11}	ε_{22}	ε_{33}	ε_{12}	ε_{13}	ε_{23}	σ_{11}	σ_{22}	σ_{33}	σ_{12}	σ_{13}	σ_{23}
Noise-free	0.041	12.59	11.68	13.54	93.82	47.67	23.48	31.34	29.50	33.02	97.56	65.54	37.41
30 dB	4.763	15.43	13.43	14.57	107.06	58.72	36.37	32.69	30.76	33.49	113.17	85.75	55.40

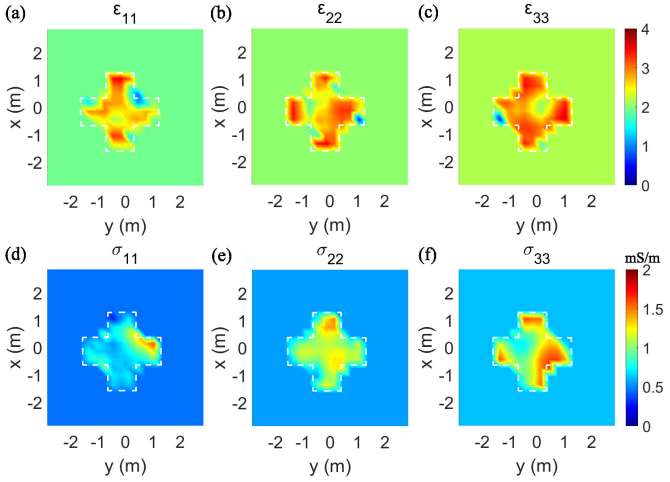

Fig. 6. 2-D xy slices of reconstructed results for the cross shape object by VBIM when SNR = 30 dB. (a)–(c) are slices at $z = 3.45$ m for the relative permittivity. (d)–(f) are slices at $z = 3.45$ m for the conductivity. The dotted boxes denote the true location of the scatterer.

and not presented here. We can see that the reconstructed shapes and dielectric parameters of the cross shape scatterer are still discernible even with 30 dB noise contamination. To quantitatively evaluate the inversion results, we introduce the data misfit and model misfit defined in [18]. The data misfits of scattered fields and model misfits of all reconstructed parameters are listed in Table II. Obviously, the model misfits become larger when the scattered field data are contaminated by noise. The model misfits of off-diagonal dielectric parameters are larger than those of the diagonal ones. This is because the background medium is constructed by rotation of the optical axis of a uniaxial anisotropic medium, which makes the off-diagonal dielectric parameters much smaller than diagonal ones. When some discretized "background" cells near the boundary of the scatterer are incorrectly judged as "scatterer" cells in the inversion, their off-diagonal dielectric parameters are assigned those of the scatterer which are much larger. As a result, the model misfits of the off-diagonal elements are significantly increased. In addition, when noise added, the scattered field misfits when the iteration terminates are a little larger than the SNR, which implies that the VBIM-SCC-SCS has a certain antinoise ability to retrieve arbitrary anisotropic objects embedded in layered arbitrary anisotropic media.

V. CONCLUSION

In this communication, we simulated the EM scattering of arbitrary anisotropic scatterers embedded in a layered arbitrary anisotropy background medium using the BCGS-FFT algorithm in the forward model. The scatterer is allowed to be placed across multiple layers. It is found that the computation complexity is increased compared with the forward scattering computation when the layered background medium is uniaxial. The reason is that the cross-coupling occurs between two types of waves at the layer boundaries of arbitrary anisotropic media, which causes the failure to decompose the layered DGFs in the z-direction. However, comparisons with FEM computation show that both the total fields and scattered fields solved by BCGS-FFT are still precise and reliable when the layered background medium is arbitrary anisotropic.

In the inversion, we reconstructed 12 dielectric parameters per cell of the arbitrary anisotropic scatterer by VBIM-SCC-SCS simultaneously. The results show that both the shape and anisotropic model parameters of the scatterer are well reconstructed. When 30 dB white Gaussian noise is added, the reconstructed shape and dielectric parameters of the scatterer are still discernible. The hybrid method VBIM-SCC-SCS is capable of dealing with the inversion of arbitrary anisotropic scatterers placed across multiple layers of an arbitrary anisotropic background medium.

REFERENCES

[1] X. Millard and Q. H. Liu, "Simulation of near-surface detection of objects in layered media by the BCGS–FFT Method," *IEEE Trans. Geosci. Remote Sens.*, vol. 42, no. 2, pp. 327–334, Feb. 2004.
[2] M. Asefi, M. Ostadrahimi, A. Zakaria, and J. Lovetri, "A 3-D dual-polarized near-field microwave imaging system," *IEEE Trans. Microw. Theory Techn.*, vol. 62, no. 8, pp. 1790–1797, Aug. 2014.
[3] K. Yang, C. Torres-Verdín, and A. E. Yılmaz, "Detection and quantification of three-dimensional hydraulic fractures with horizontal borehole resistivity measurements," *IEEE Trans. Geosci. Remote Sens.*, vol. 53, no. 8, pp. 4605–4615, Aug. 2015.

[4] Z. Q. Zhang and Q. H. Liu, "Three-dimensional nonlinear image reconstruction for microwave biomedical imaging," *IEEE Trans. Biomed. Eng.*, vol. 51, no. 3, pp. 544–548, Mar. 2004.

[5] C. Yu *et al.*, "Active microwave imaging II: 3-D system prototype and image reconstruction from experimental data," *IEEE Trans. Microw. Theory Techn.*, vol. 56, no. 4, pp. 991–1000, Apr. 2008.

[6] Z. Q. Zhang, Q. H. Liu, C. Xiao, E. Ward, G. Ybarra, and W. T. Joines, "Microwave breast imaging: 3-D forward scattering simulation," *IEEE Trans. Biomed. Eng.*, vol. 50, no. 10, pp. 1180–1189, Oct. 2003.

[7] K. A. Michalski and J. R. Mosig, "Multilayered media Green's functions in integral equation formulations," *IEEE Trans. Antennas Propag.*, vol. 45, no. 3, pp. 508–519, Mar. 1997.

[8] X. Millard and Q. H. Liu, "A fast volume integral equation solver for electromagnetic scattering from large inhomogeneous objects in planarly layered media," *IEEE Trans. Antennas Propag.*, vol. 51, no. 9, pp. 2393–2401, Sep. 2003.

[9] K. Yang and A. E. Yılmaz, "A three-dimensional adaptive integral method for scattering from structures embedded in layered media," *IEEE Trans. Geosci. Remote Sens.*, vol. 50, no. 4, pp. 1130–1139, Apr. 2012.

[10] L.-P. Song, S. D. Billings, L. R. Pasion, and D. W. Oldenburg, "Transient electromagnetic scattering of a metallic object buried in underwater sediments," *IEEE Trans. Geosci. Remote Sens.*, vol. 54, no. 2, pp. 1091–1102, Feb. 2016.

[11] G. Li, H. Cai, and C.-F. Li, "Alternating joint inversion of controlled-source electromagnetic and seismic data using the joint total variation constraint," *IEEE Trans. Geosci. Remote Sens.*, vol. 57, no. 8, pp. 5914–5922, Aug. 2019.

[12] C. J. Leuschen and R. G. Plumb, "A matched-filter-based reverse-time migration algorithm for ground-penetrating radar data," *IEEE Trans. Geosci. Remote Sens.*, vol. 39, no. 5, pp. 929–936, May 2001.

[13] L. Li, W. Zhang, and F. Li, "A novel autofocusing approach for real-time through-wall imaging under unknown wall characteristics," *IEEE Trans. Geosci. Remote Sens.*, vol. 48, no. 1, pp. 423–431, Jan. 2010.

[14] K. Yang and A. E. Yılmaz, "FFT-accelerated analysis of scattering from complex dielectrics embedded in uniaxial layered media," *IEEE Geosci. Remote Sens. Lett.*, vol. 10, no. 4, pp. 662–666, Jul. 2013.

[15] F. Han, J. Zhuo, N. Liu, Y. Liu, H. Liu, and Q. H. Liu, "Fast solution of electromagnetic scattering for 3-D inhomogeneous anisotropic objects embedded in layered uniaxial media by the BCGS-FFT method," *IEEE Trans. Antennas Propag.*, vol. 67, no. 3, pp. 1748–1759, Mar. 2019.

[16] Y. Zhong, P.-P. Ding, M. Lambert, D. Lesselier, and X. Chen, "Fast calculation of scattering by 3-D inhomogeneities in uniaxial anisotropic multilayers," *IEEE Trans. Antennas Propag.*, vol. 62, no. 12, pp. 6365–6374, Dec. 2014.

[17] J. Zhuo, L. Ye, F. Han, L. Xiong, and Q. H. Liu, "Multiparametric electromagnetic inversion of 3-D biaxial anisotropic objects embedded in layered uniaxial media using VBIM enhanced by structural consistency constraint," *IEEE Trans. Antennas Propag.*, to be published.

[18] J. Li, J. Zhuo, Z. Guan, F. Han, and Q. H. Liu, "3-D electromagnetic scattering and inverse scattering by magnetodielectric objects with arbitrary anisotropy in layered uniaxial media," *IEEE Trans. Antennas Propag.*, vol. 68, no. 2, pp. 1009–1022, Feb. 2020.

[19] G. L. Wang, T. Barber, P. Wu, D. Allen, and A. Abubakar, "Fast inversion of triaxial induction data in dipping crossbedded formations," *Geophysics*, vol. 82, no. 2, pp. D31–D45, Mar. 2017.

[20] S. Liu, J. Mo, and N. Yuan, "Research on the relation between the unmagnetized plasma density and the stealth of target," *J. Radio Sci.*, vol. 18, no. 1, pp. 57–61, Feb. 2003.

[21] F. Han, B. Liang, J. Li, F. Liu, G. Lu, and Q. H. Liu, "Mid- and low-latitude ionospheric D region remote sensing by radio atmospherics—Part I: Forward modeling and field measurement validations," *IEEE Trans. Antennas Propag.*, vol. 68, no. 2, pp. 1044–1054, Feb. 2020.

[22] A. Abubakar, P. Van Den Berg, and J. Mallorqui, "Imaging of biomedical data using a multiplicative regularized contrast source inversion method," *IEEE Trans. Microw. Theory Techn.*, vol. 50, no. 7, pp. 1761–1771, Jul. 2002.

[23] X. Chen, "Subspace-based optimization method for solving inverse-scattering problems," *IEEE Trans. Geosci. Remote Sens.*, vol. 48, no. 1, pp. 42–49, Jan. 2010.

[24] Y. M. Wang and W. C. Chew, "An iterative solution of the two-dimensional electromagnetic inverse scattering problem," *Int. J. Imag. Syst. Technol.*, vol. 1, no. 1, pp. 100–108, Mar. 1989.

[25] J. Zhuo, F. Han, L. Ye, Z. Yu, and Q. H. Liu, "Simulation of electromagnetic scattering of 3-D inhomogeneous biaxial anisotropic magnetodielectric objects embedded in uniaxial anisotropic media by the mixed-order BCGS-FFT method," *IEEE Trans. Microw. Theory Techn.*, vol. 66, no. 8, pp. 3745–3755, Aug. 2018.

[26] Y. Hu, Y. Fang, D. Wang, Y. Zhong, and Q. H. Liu, "Electromagnetic waves in multilayered generalized anisotropic media," *IEEE Trans. Geosci. Remote Sens.*, vol. 56, no. 10, pp. 5758–5766, Oct. 2018.